

Quantum elliptic vortex in a nematic-spin Bose-Einstein condensate

Hiromitsu Takeuchi*

*Department of Physics and Nambu Yoichiro Institute of Theoretical and Experimental Physics (NITEP),
Osaka City University, Osaka 558-8585, Japan*

(Dated: October 16, 2020)

A novel topological defect in a spin-nematic superfluid is found theoretically. A quantized vortex spontaneously breaks its axisymmetry, leading to an elliptic vortex in nematic-spin Bose-Einstein condensates with small positive quadratic Zeeman effect. The new vortex is considered the Joukowski transform of a conventional vortex. Its oblateness grows when the Zeeman length scale exceeds the spin healing length. This structure is sustained by balancing the hydrodynamic potential and the elasticity of a soliton connecting two spin spots, which are observable by *in situ* magnetization imaging. The findings suggest that non-equilibrium dynamics of the quark-hadron transition can be simulated in the nematic-spin superfluid according to a similarity between the quark confinement by gluons and the spin-spot confinement by the soliton.

Topological defects (TDs) caused by spontaneous symmetry breaking (SSB) phase transition is ubiquitous, existing as skyrmions in spintronic devices [1], vortices in superconductors/superfluids [2, 3], and even disclinations in LCD displays [4]. Thanks to the universal concept of SSB, TDs in laboratories are useful to simulating TDs in other exotic settings, the early universe, the dense matters in compact stars, higher-dimensional spacetimes in field theory [5–8]. Multi-component superfluids with spin freedom, such as spin-triplet superfluid ^3He and binary/spinor Bose-Einstein condensates (BECs) [9–12], are powerful tools to develop theories of TDs since various TDs are realized there. Such superfluids are called the nematic-spin superfluids [13], whose order state is partly represented by a vector $\hat{\mathbf{d}}$ that mimics the *director* $\hat{\mathbf{d}}$ in nematic liquid crystals (NLCs) [4].

Nematic-spin superfluids support not only conventional TDs in NLCs (disclination, hedgehog, domain wall, and boojum [14–24]), but also novel TDs combined with the superfluidity, e.g., half quantum vortex (HQV) [25]. The simplest type of HQV has been realized experimentally in different superfluids [26–28], where the core of a vortex in a spin component is occupied by other components. A nontrivial HQV is terminated by a domain wall across which the order-parameter phase jumps by π . The wall-HQV composites were first realized as the double-core vortices in $^3\text{He-B}$ [29] and revisited [30–32], motivated by the early-universe scenario nucleating the composites of the Kibble-Lazarides-Shafi (KLS) walls and cosmic strings [33–35]. Recently, the nonequilibrium dynamics of wall-HQV composites was observed in phase transition from the antiferromagnetic (AF) phase to the polar (P) phase in a spin-1 ^{23}Na BEC [36, 37]. However, the dynamics are poorly understood, because of the lack knowledge about properties of wall-HQV composites. Determining these properties is important for understanding KLS-wall-HQV composites and double-core vortices in $^3\text{He-B}$ [38–42]), the Berezinskii-Kosterlitz-Thouless transition in spinor BECs [43–45], and even the quark-confinement problem in hadronic physics con-

nected with the vortex-confinement problem [46–49].

Here, it is theoretically shown that a wall-HQV composite in spin-1 BECs [36, 37] takes an exotic state in equilibrium with small positive quadratic Zeeman effect. This state, called the elliptic vortex, is hydrodynamically considered the Joukowski transform of a conventional vortex and has an elliptic structure with spin spots (Fig. 1). The spots are confined to the elliptic vortex core and stabilized by a balance between the hydrodynamic effect and the tension of a domain wall or a soliton spanned between the spots. The finding suggests that the quark-hadron transition in the early universe or the ‘Little Bang’ [50, 51] can be simulated in ultra-cold atoms.

Formulation— A spin-1 BEC is described by the condensate wave function Φ_m ($m = 0, \pm 1$) of the $|m\rangle$ Zeeman component in the Gross-Pitaevskii model [12, 52]. The thermodynamic energy is represented as $G(\{\Phi_m\}) = \int d^3x \mathcal{G}$, with $\mathcal{G} = \frac{\hbar^2}{2M} \sum_m |\nabla \Phi_m|^2 + \mathcal{U}$, and

$$\mathcal{U} = \frac{c_0}{2} n^2 + \frac{c_2}{2} \mathbf{s}^2 - (\mu - q)n - q |\Phi_0|^2 - p s_z. \quad (1)$$

Here, we introduced the chemical potential $\mu (> 0)$ and the coefficient q (p) of the quadratic (linear) Zeeman effect. In the Cartesian representation $\Phi = [\Phi_x, \Phi_y, \Phi_z]^T = \left[\frac{-1}{\sqrt{2}}(\Phi_{+1} - \Phi_{-1}), \frac{i}{\sqrt{2}}(\Phi_{+1} + \Phi_{-1}), \Phi_0 \right]^T$ [53], the condensate density is expressed by the dot product $n = \sum_m |\Phi_m|^2 = \Phi^* \cdot \Phi$ and the spin density by the cross product $\mathbf{s} = [s_x, s_y, s_z]^T = i \Phi \times \Phi^*$.

The ground (bulk) state is obtained by minimizing $U = \int d^3x \mathcal{U}$. Assuming $c_2 = 0.016c_0 > 0$ with $p = 0$ obtained experimentally [36, 37], the ground state has no magnetization ($\mathbf{s} = 0$), and we have

$$\Phi = \sqrt{n} e^{i\theta_G} \hat{\mathbf{d}}. \quad (2)$$

The real unit vector $\hat{\mathbf{d}} = [d_x, d_y, d_z]^T$ is the *pseudo*-director; an ordered state of $(\hat{\mathbf{d}}, \theta_G)$ is identical to that of $(-\hat{\mathbf{d}}, \theta_G + \pi)$. The ground state in the P (AF) phase with $q > 0$ ($q < 0$) is represented as $n = n_P$ and $\hat{\mathbf{d}} = \pm \hat{\mathbf{z}}$

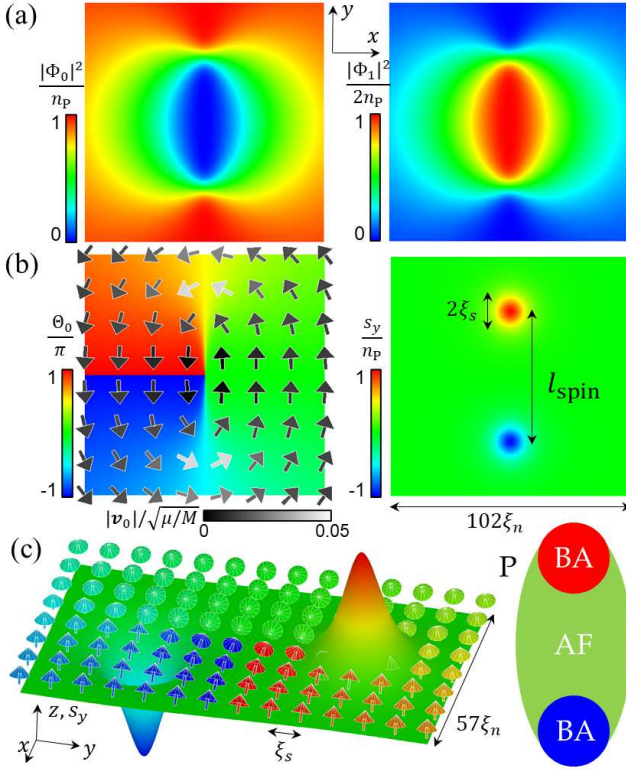


FIG. 1. The cross-sectional profile of an elliptic vortex for $q/\mu = 2^{-17} \approx 7.6 \times 10^{-6}$. (a) The left and right panels show the profiles of $\frac{|\Phi_0|^2}{n_P}$ and $\frac{|\Phi_1|^2}{2n_P}$, respectively. The density $|\Phi_{-1}|^2$ (not shown) is the same as $|\Phi_1|^2$. (b) The vector field on the left shows $\mathbf{v}_0 = \frac{\hbar}{M} \nabla \Theta_0$, with the background plot of $\Theta_0 = \arg \Phi_0$. The phase $\arg \Phi_{\pm 1}$ is homogeneous inside the core (not shown). The spin density s_y is plotted on the right, while $s_x = s_z = 0$. (c) (Left) The texture of the unit vector $\mathbf{d}/|\mathbf{d}|$ (arrow) in Eq. (2). The color of the arrows and the surface correspond to Θ_0 and s_y in (b), respectively. (Right) A schematic of the cross-sectional profile.

($n = n_{\text{AF}}$ and $\hat{\mathbf{d}} = \hat{\mathbf{r}}_{\perp}$) with the bulk density $n_P = \frac{\mu}{c_0}$ ($n_{\text{AF}} = \frac{\mu - q}{c_0}$), and the unit vector $\hat{\mathbf{z}}$ ($\hat{\mathbf{r}}_{\perp}$) parallel (normal) to the quantization axis. By rescaling energy and length by μ and $\xi_n \equiv \frac{\hbar}{\sqrt{M\mu}}$, respectively, the P phase is parameterized by two dimensionless quantities, $\frac{c_2}{c_0}$ and $\frac{q}{\mu}$.

Vortex core structure— One might expect that there is nothing strange about the occurrence of vortices in P phase, whose order parameter is a complex scalar $\Phi_0 = \sqrt{n_P} e^{i\Theta_0}$ with $\Phi_{\pm 1} = 0$, as in conventional superfluids. However, the vortex core can be unconventional in nematic-spin superfluids; the core of the TDs is occupied by different ordered states so as to reduce the energy. Similarly, the vortex core can be occupied by the $m = \pm 1$ component in the P phase.

To examine the conjecture, the lowest-energy solution was obtained by numerically minimizing G in the steepest descent method [54]. It is found that a non-

axisymmetric core structure is observed for small q/μ . Figure 2 shows the typical cross-sectional profile of the vortex for $\frac{q}{\mu} = 2^{-17}$ in a box potential [55]. The vortex core is occupied by the $m = \pm 1$ components, and the density n is mostly homogeneous [Fig. 1(a)]. Surprisingly, the velocity field forms an elliptic structure, and two spin spots are observed with opposite transverse magnetization ($s_y \neq 0$) at the edges of the core [Fig. 1(b)].

The distance l_{spin} between the spin spots is a decreasing function of q [Fig. 2(a)]. Accordingly, the density n_{core} at the center of the vortex core and the maximum spin density s_{\perp}^{max} decrease with q and vanish at a critical value $q_C \approx 0.25\mu$ [Fig. 2(b)] [56, 57]. This behavior is similar to that of the AF-core soliton [58], where the soliton core is vacant for large q but occupied by the AF state ($\mathbf{s} = 0$ with $\Phi_{\pm 1} \neq 0$ and $\Phi_0 \approx 0$) for small q . In our case, however, the vortex core is occupied by two different states, the Broken-axisymmetry (BA) state ($\mathbf{s} \perp \hat{\mathbf{z}}$ with $\Phi_1 \Phi_0 \Phi_{-1} \neq 0$) and the AF state.

To explain the core structure schematically, it is useful to introduce a representation

$$\Phi = e^{i\Theta_0} (\mathbf{d} + i\mathbf{e}) \quad (3)$$

with $\mathbf{d} = [d_x, d_y, d_z]^T$ with $d_z \geq 0$ and $\mathbf{e} \perp \hat{\mathbf{z}}$. Equation (3) reduces Eq. (2) for $\mathbf{s} = 2\mathbf{d} \times \mathbf{e} = 0$ with $\mathbf{d} = \sqrt{n}\hat{\mathbf{d}}$. The left panel in Fig 1(c) shows a cross-sectional plot of $\frac{\mathbf{d}}{|\mathbf{d}|}$ and s_y . In the region between the spin spots, \mathbf{d} lies on the xy -plane forming the AF state, where the state $(\hat{\mathbf{d}}, \Theta_0) = (-\hat{\mathbf{x}}, \pm\pi)$ for $x > 0$ is identical to $(\hat{\mathbf{x}}, 0)$ for $x < 0$ along the yz -plane. The nematic-spin order is destroyed when $\hat{\mathbf{d}}$ is ill-defined in the spin spots occupied by the BA state [see the right panel in Fig 1(c)].

To clarify our problem, the main goal is to answer the following two questions;

Q1: What causes the axisymmetry breaking?

Q2: What is the physical mechanism to stabilize the elliptic structure?

Vortex winding rule— As the answer for the first question, it is claimed that the spin interaction breaks the axisymmetry. To justify the claim logically, we introduce a winding rule of an axisymmetric vortex in spin-1 BECs. We consider a straight vortex along the z -axis, the cross section of which is axisymmetric as $\Phi_m = f_m(r) e^{iL_m\varphi}$, with radius $r = \sqrt{x^2 + y^2}$, and azimuthal angle φ in cylindrical coordinates. The rule states that L_m is parameterized by the winding numbers L and N , associated with the mass- and spin-current, respectively, and given by

$$L_m = L + mN \quad (L, N = 0, \pm 1, \pm 2, \dots). \quad (4)$$

This rule is applicable only when the real functions $f_m(r)$ ($m = 0, \pm 1$) are nonzero [59].

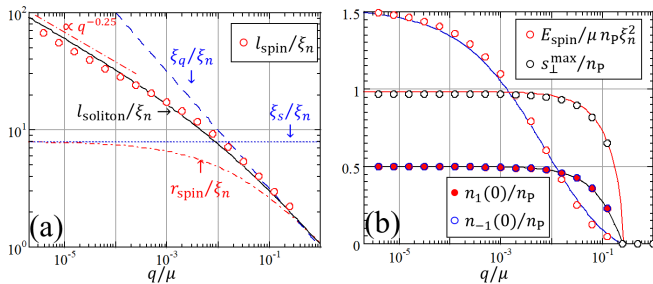


FIG. 2. (a) The q -dependence of l_{spin} . The solid curve represents the evaluation by Eq. (12). All lengths are rescaled by ξ_n . (b) The q -dependence of the spin interaction E_{spin} , the maximum spin density $s_{\perp}^{\text{max}} = \max(s_y)$, and the core density $n_{\pm 1}(0)$. The solid curve tracing each data corresponds to an analytic formula (see text).

By contraposition of the above argument, the vortex must be non-axisymmetric, when the winding rule is not satisfied. As seen in Fig. 1, only the $m = 0$ component has a nonzero winding number, corresponding to $L_0 = 1$ and $L_{\pm 1} = 0$. Such a set of winding numbers cannot satisfy the winding rule. The axisymmetry is exactly recovered only for $\Phi_{\pm 1} = 0$ ($q \geq q_C$).

The spin interaction is essential to the axisymmetry breaking. The energy terms other than the spin interaction in Eq. (1) have a quadratic dependence on the order parameter given by $|\Phi_m|^2 \rightarrow f_m^2$. The winding rule is directly connected with the transverse spin density while $s_z = |\Phi_1|^2 - |\Phi_{-1}|^2$. This is the reason why the spin spots exhibit transverse magnetization. The orientations of the transverse spin and the axes of the elliptic structure depend on the phases $\arg \Phi_m$.

Joukowski mapping— To answer the second question, the potential flow theory in two-dimensional flow is extended to our problem. The elliptic core structure hints at the Joukowski transformation [60], since the velocity field on the cross-section is considered a two-dimensional potential flow. This perception is the motivation for investigating the problem, and the following analysis lead to a quantitative evaluation of the core structure.

The velocity field $\mathbf{v}_0 = \frac{\hbar}{M} \nabla \Theta_0 = (u, v)$ in the xy -plane is generated by a conformal mapping called the Joukowski transformation from a vortex within a cylinder of radius a in the ζ complex plane to the xy -plane, $x + iy = \zeta + \frac{a^2}{\zeta}$ [60]. By using the parameterization $\zeta = ia e^{\phi + i\psi}$ ($\phi \geq 0$), one obtains $(x, y) = 2a(\cosh \phi \cos(\psi + \pi), \sinh \phi \sin(\psi + \pi))$, representing an ellipse of width $4a \cosh \phi$ and thickness $4a \sinh \phi$.

The velocity field is computed by applying the conformal mapping to the complex velocity potential W of the vortex in the ζ -plane,

$$W = -i \frac{\kappa}{2\pi} \log \zeta. \quad (5)$$

The circulation $\kappa = \frac{2\pi\hbar}{M}$ around a quantized vortex is

conserved in the transformation as follows. By applying the transformation to Eq. (5) and using the formula $v \rightarrow \pm \frac{\kappa}{2\pi} \frac{1}{\sqrt{4a^2 - y^2}}$ for $|y| < 2a$ in the limit $x \rightarrow \pm 0$, the vorticity $\omega_z(x, y) = (\nabla \times \mathbf{v}_0)_z$ forms a segment singularity of width $4a$,

$$\omega_z(\mathbf{r}) = \frac{\kappa}{\pi} \frac{1}{\sqrt{4a^2 - y^2}} \delta(x) \Theta(2a - |y|). \quad (6)$$

with the step function Θ ($\Theta = 1$ for $2a \geq |y|$ and $\Theta = 0$ for $2a < |y|$). By integrating Eq. (6), it is confirmed that the circulation is conserved as $\int dx dy \omega_z = \kappa$.

Hydrodynamic potential— To reveal the physical mechanism that stabilizes the elliptic vortex, the energy E_{vortex} of a vortex of unit length is evaluated. The vortex energy in the ζ -plane is computed conventionally by considering the contribution from the core region ($|\zeta| < \rho_{\text{core}} \equiv a e^{\phi_{\text{core}}}$) and the outer region ($|\zeta| > \rho_{\text{core}}$) separately [3]. Similarly, we consider the Joukowski mapping of the former and the latter, corresponding to an ellipse of area S_{core} and outer area S_{out} in the xy -plane, respectively.

The core region is characterized by two parameters a and $r_{\text{core}} \equiv \rho_{\text{core}} - a$ as

$$S_{\text{core}} = \pi R_+ R_- = \pi \frac{(a + r_{\text{core}})^4 - a^4}{(a + r_{\text{core}})^2}, \quad (7)$$

with $R_{\pm} = \frac{(a + r_{\text{core}})^2 \pm a^2}{a + r_{\text{core}}}$. Here, $2R_{+(-)}$ is the width (thickness) of the ellipse. For high oblateness with $\frac{a}{r_{\text{core}}} \gg 1$, we have $R_+ \approx 2a$ and $R_- \approx 2r_{\text{core}}$. The axisymmetric limit $\frac{a}{r_{\text{core}}} \rightarrow 0$ results in $R_+ = R_- \rightarrow r_{\text{core}}$.

The vortex energy is defined as the excess energy in the presence of the vortex, with respect to the bulk energy $E_{\text{bulk}} = \mathcal{U}_P(S_{\text{in}} + S_{\text{out}})$ with energy density $\mathcal{U}_P = -\frac{1}{2} \mu n_P$ of the P state. The vortex energy is then represented formally by

$$E_{\text{vortex}} = E_{\text{out}} + E_{\text{core}} - E_{\text{bulk}} = U_{\text{core}} + U_{\text{out}} \quad (8)$$

with $E_{\text{core(out)}} = \int_{S_{\text{core(out)}}} dx dy \mathcal{G}$ and $U_{\text{core(out)}} = E_{\text{core(out)}} - \mathcal{U}_P S_{\text{core(out)}}$. The potential U_{out} of the outer region is evaluated by computing the integral in E_{out} analytically with an approximation $n \approx n_P \left(1 - \frac{M}{2\mu} v_0^2\right)$, where the quantum pressure is neglected. In the approximation up to the order of $\mathcal{O}\left(\frac{M}{2\mu} v_0^2\right)$, a straightforward computation yields

$$U_{\text{out}} \approx U_{\text{hyd}} = \frac{M n_P \kappa^2}{4\pi} \ln \frac{R}{a + r_{\text{core}}}. \quad (9)$$

Here, we used the radius $R = a e^{\phi_{\text{out}}}$ of the system boundary by assuming $R \gg a$ [61].

Elastic core potential— The core potential U_{core} is determined by introducing a phenomenological model, where a soliton is spanned between the spin spots. This model is justified by the fact that the phase gradient is

mainly concentrated around the spin spots, consistent with the vorticity distribution (6) [see also Fig. 1(c)]; thus, the core structure between the spots is similar to that of the AF-core soliton [58]. Accordingly, we write

$$U_{\text{core}} = E_{\text{soliton}} + E_{\text{spin}} \quad (10)$$

where the soliton energy E_{soliton} is a function of the soliton length $l_{\text{soliton}} \sim l_{\text{spot}}$ and the spin interaction E_{spin} comes from the second term of Eq. (1).

The spin interaction is determined independently from the hydrodynamic argument, and thus U_{core} depends explicitly on l_{spot} through E_{soliton} . The size r_{spin} and the magnitude $s_{\perp}^{\text{max}} = \max(s_y)$ of the spin spot are asymptotic to $\xi_s = \frac{\hbar}{\sqrt{Mc_2 n_P}}$ and n_P , respectively, for $\xi_q \gg \xi_s \gg \xi_n$. For $\xi_s \gg \xi_q \gtrsim \xi_n$, the core density grows as $n_{\pm 1}(0) \propto 1 - \frac{q}{q_C}$ in the continuous phase transition [62], and the size r_{spin} must be bounded below the vortex core size $\lesssim \xi_q$. Therefore, the size of a spin spot is simply parameterized as

$$r_{\text{spin}}^{-1} = \xi_s^{-1} + C_{\text{spin}} \xi_q^{-1} \quad (11)$$

with $C_{\text{spin}} \sim \mathcal{O}(1)$. In fact, the spin interaction, estimated by $E_{\text{spin}} = \frac{1}{2} c_2 (s_y^{\text{max}})^2 \pi r_{\text{spin}}^2$ agrees well with the numerical result with $C_{\text{spin}} = 0.8$ [Fig. 2 (b)] [63].

To simplify the analysis, we write as $l_{\text{soliton}} \equiv 4a + 4r_{\text{core}}$. The equilibrium length is then determined by $\frac{\partial}{\partial l_{\text{soliton}}} E_{\text{vortex}} = \frac{\partial}{\partial l_{\text{soliton}}} (U_{\text{hyd}} + E_{\text{soliton}}) = 0$. In the first approximation, the soliton energy E_{soliton} is expressed as $E_{\text{soliton}}^{\text{1st}} = \alpha_{\text{AF}} l_{\text{soliton}}$ with the tension coefficient $\alpha_{\text{AF}} \sim \sqrt{q \mu n_P} \xi_n$ of the AF-core soliton [58]. This approximation fails for $\xi_q \gg \xi_s$. Actually, the thickness of the elliptic core is much smaller than the thickness $\sim \xi_q$ of the AF-core soliton forming a halo structure [Fig. 1 (a)], which increases the tension effectively. To take this effect into account, we introduce a phenomenological formula

$$\frac{E_{\text{soliton}}}{\mu n_P \xi_n^2} = \sqrt{\frac{q}{\mu}} \frac{l_{\text{soliton}}}{\xi_n} \left(1 + \frac{l_{\text{soliton}}}{r_{\text{spin}}} \right). \quad (12)$$

This formula yields $\frac{l_{\text{soliton}}}{\xi_n} = \frac{r_{\text{spin}}}{4\xi_n} \left(\sqrt{1 + 8\pi \frac{\xi_q}{r_{\text{spin}}} - 1} \right)$, and explains the scaling behavior $l_{\text{soliton}} \sim l_{\text{spin}} \propto q^{-0.25}$ for $\xi_q \gg \xi_s$ in Fig. 2(a). This means that the soliton is effectively elastic with $E_{\text{soliton}} \propto l_{\text{soliton}}^2$ for $l_{\text{spin}} \gg r_{\text{spin}}$.

Rotating solutions— Finally, the response to an external rotation is investigated as a dynamical property. The external rotation of angular frequency Ω is described by the energy in the rotating frame, $G' = G - \Omega L_z$ with the angular momentum L_z along the z -axis [64]. The width l_{spin}^{Ω} of an elliptic vortex decreases with Ω [Fig. 3(a)], since the angular momentum increases more as the vorticity is localized more toward the center. Owing to the boundary effect [65], the single-vortex states are unstable for large $|\Omega|$ or small q/μ , leading to a lattice of elliptic vortices [inset of Fig. 3(a)].

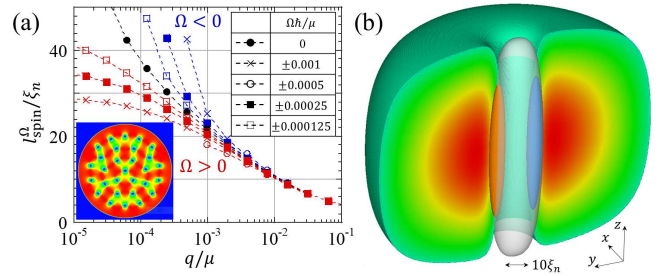


FIG. 3. (a) The q -dependence of the width l_{spin}^{Ω} of a rotating elliptic vortex with angular velocity Ω . The single vortex is unstable for larger $|\Omega|$ and smaller q due the boundary effect. The inset shows an elliptic-vortex lattice obtained after the instability due to the boundary effect for $\Omega \hbar/\mu = 0.001$ and $q/\mu = 2^{-11}$. (b) The three dimensional solution of an elliptic vortex in a harmonic trap for $\Omega \hbar/\mu = 0.0005$. The isovolume plot shows the region $|\Psi_0|^2 c_0/\mu \leq 0.3$ for $x > 0$ with its $x = 0$ cross-section profile. A translucent surface along the z -axis represents the isosurface of $|\Psi_{\pm 1}|^2 c_0/\mu = 0.15$, to which the two poles of the isosurfaces $s_y c_0/\mu = \pm 0.7$ are attached (red for positive and blue for negative).

The three-dimensional structure of an elliptic vortex is demonstrated numerically for a feasible setup in Fig. 3(b). A ^{23}Na BEC of 5.6×10^5 atoms is in a harmonic trap $V_{\text{trap}} = \frac{M}{2} (\omega_{\perp}^2 r^2 + \omega_z^2 z^2)$ with $\frac{\hbar}{\mu} (\omega_{\perp}, \omega_z) \approx (0.019, 0.024)$. The spin spots appear as two poles (red and blue) along the $m = \pm 1$ component (translucent pole) in the vortex core.

Discussion— Although the wall-HQV composites were thought to be finally unstable by the snake instability in Refs. [36, 37], the result suggests that they survive as elliptic vortices after the phase transition. The vortices including their dynamics will be observed through the transverse-spin spots by *in situ* magnetization imaging [27]. The theory here can be applied in a similar manner to the double-core vortex or the KLS-wall-HQV composite in $^3\text{He-B}$, while different forms of the hydrodynamic potential and soliton tension were introduced [66].

It should be mentioned that similar composite objects are investigated experimentally as the spin-mass vortex attached by a planar soliton in $^3\text{He-B}$ [67, 68] and theoretically as the vortex molecules in Rabi-coupled binary BECs [46–49, 69–73]. Interestingly, the confinement of vortices by domain walls is considered a toy model of the quark-confinement problem as was originally suggested by Son and Stephanov [46]. Accordingly, “HQV-wall plasma”, an analog of quark-gluon plasma (QGP), occurs at a finite temperature T at least for $T > \frac{q}{k_B}$ in nematic-spin BECs, where thermal fluctuations free the spin spots from the confinement by the AF-core soliton. In this sense, the observed phase-transition dynamics [36, 37] are regarded as simulations of the transition dynamics from QGP to hadrons like the Big-Bang simulation in ‘Little Bang’ [51]. Further investigations on the dynamics and interactions of elliptic vortices will shed light on

unexplored phase-transition dynamics in different physical systems.

H.T. thanks Yong-il Shin for discussion and critical reading of the manuscript. This work is supported by JSPS KAKENHI Grant Numbers JP17K05549, JP18KK0391, JP20H01842, and in part by the OCU "Think globally, act locally" Research Grant for Young Scientists 2019 and 2020 through the hometown donation fund of Osaka City.

-
- * takeuchi@osaka-cu.ac.jp; <http://hiromitsu-takeuchi.appspot.com>
- [1] Roland Wiesendanger. Nanoscale magnetic skyrmions in metallic films and multilayers: a new twist for spintronics. *Nature Reviews Materials*, 1(7):1–11, 2016.
 - [2] David R Tilley. *Superfluidity and superconductivity*. Routledge, 2019.
 - [3] Russell J Donnelly. *Quantized vortices in helium II*, volume 2. Cambridge University Press, 1991.
 - [4] S. Chandrasekhar. *Liquid Crystals*. Cambridge University Press, 2 edition, 1992.
 - [5] Alexander Vilenkin and E Paul S Shellard. *Cosmic strings and other topological defects*. Cambridge University Press, 2000.
 - [6] Dany Page and Sanjay Reddy. Dense matter in compact stars: theoretical developments and observational constraints. *Annu. Rev. Nucl. Part. Sci.*, 56:327–374, 2006.
 - [7] Tanmay Vachaspati. *Kinks and domain walls: An introduction to classical and quantum solitons*. Cambridge University Press, 2006.
 - [8] ASHOK SEN. Tachyon dynamics in open string theory. *International Journal of Modern Physics A*, 20(24):5513–5656, 2005.
 - [9] Dieter Vollhardt and Peter Wolffe. *The superfluid phases of helium 3*. Courier Corporation, 2013.
 - [10] Grigory E Volovik. *The universe in a helium droplet*, volume 117. Oxford University Press on Demand, 2003.
 - [11] Kenichi Kasamatsu, Makoto Tsubota, and Masahito Ueda. Vortices in multicomponent Bose–Einstein condensates. *International Journal of Modern Physics B*, 19(11):1835–1904, 2005.
 - [12] Yuki Kawaguchi and Masahito Ueda. Spinor Bose–Einstein Condensates. *Physics Reports*, 520(5):253–381, 2012.
 - [13] The term "nematic-spin" or "spin-nematic" has been also used in the literatures of different condensed matter systems, e.g., the spin-nematic phase in antiferromagnets [Hirokazu Tsunetsugu and Mitsuhiro Arikawa, *Spin Nematic Phase in S=1 Triangular Antiferromagnets*, *J. Phys. Soc. Jpn.* **75**, 083701 (2006)] and the nematic-spin fluid in BaFe₂As₂ [L. W. Harriger, H. Q. Luo, M. S. Liu, C. Frost, J. P. Hu, M. R. Norman, and Pengcheng Dai, *Nematic spin fluid in the tetragonal phase of BaFe₂As₂*, *Phys. Rev. B* **84**, 054544 (2011)].
 - [14] N. D. Mermin. The topological theory of defects in ordered media. *Rev. Mod. Phys.*, 51:591–648, Jul 1979.
 - [15] PB Sunil Kumar and GS Ranganath. On certain liquid crystal defects in a magnetic field. *Molecular Crystals and Liquid Crystals*, 177(1):131–144, 1989.
 - [16] Grigory E Volovik. *Exotic properties of superfluid ³He*, volume 1. World Scientific, 1992.
 - [17] V. P. Mineyev and G. E. Volovik. Planar and linear solitons in superfluid ³He. *Phys. Rev. B*, 18:3197–3203, Oct 1978.
 - [18] Fei Zhou. Spin Correlation and Discrete Symmetry in Spinor Bose-Einstein Condensates. *Phys. Rev. Lett.*, 87:080401, Aug 2001.
 - [19] Fei Zhou. Quantum spin nematic states in Bose–Einstein condensates. *International Journal of Modern Physics B*, 17(14):2643–2698, 2003.
 - [20] J. Ruostekoski and J. R. Anglin. Monopole Core Instability and Alice Rings in Spinor Bose-Einstein Condensates. *Phys. Rev. Lett.*, 91:190402, Nov 2003.
 - [21] N. D. Mermin. *Surface Singularities and Superflow in ³He-A*, pages 3–22. Springer US, Boston, MA, 1977.
 - [22] GE Volovik. Defects at interface between A and B phases of superfluid ³He. *JETP Lett*, 51(8), 1990.
 - [23] T Sh Misirpashaev. The topological classification of defects at a phase interface. *Soviet physics, JETP*, 72(6):973–982, 1991.
 - [24] Hiromitsu Takeuchi and Makoto Tsubota. Boojums in rotating two-component Bose-Einstein condensates. *Journal of the Physical Society of Japan*, 75(6):063601, 2006.
 - [25] U. Leonhardt and G.E. Volovik. How to create Alice string (half quantum vortex) in a vector Bose-Einstein condensate. *Pisma Zh. Eksp. Teor. Fiz.*, 72:66–70, 2000.
 - [26] M. R. Matthews, B. P. Anderson, P. C. Haljan, D. S. Hall, C. E. Wieman, and E. A. Cornell. Vortices in a Bose-Einstein Condensate. *Phys. Rev. Lett.*, 83:2498–2501, Sep 1999.
 - [27] Sang Won Seo, Seji Kang, Woo Jin Kwon, and Yong-il Shin. Half-Quantum Vortices in an Antiferromagnetic Spinor Bose-Einstein Condensate. *Phys. Rev. Lett.*, 115:015301, Jul 2015.
 - [28] S. Autti, V. V. Dmitriev, J. T. Mäkinen, A. A. Soldatov, G. E. Volovik, A. N. Yudin, V. V. Zavjalov, and V. B. Eltsov. Observation of Half-Quantum Vortices in Topological Superfluid ³He. *Phys. Rev. Lett.*, 117:255301, Dec 2016.
 - [29] Y. Kondo, J. S. Korhonen, M. Krusius, V. V. Dmitriev, Y. M. Mukharsky, E. B. Sonin, and G. E. Volovik. Direct observation of the nonaxisymmetric vortex in superfluid ³He-B. *Phys. Rev. Lett.*, 67:81–84, Jul 1991.
 - [30] JT Mäkinen, VV Dmitriev, Jaakko Nissinen, Juho Rysti, GE Volovik, AN Yudin, Kuang Zhang, and VB Eltsov. Half-quantum vortices and walls bounded by strings in the polar-distorted phases of topological superfluid ³He. *Nature communications*, 10(1):1–8, 2019.
 - [31] G. E. Volovik and K. Zhang. String monopoles, string walls, vortex skyrmions, and nexus objects in the polar distorted B phase of ³He. *Phys. Rev. Research*, 2:023263, Jun 2020.
 - [32] K Zhang. One dimensional nexus objects, network of Kibble-Lazarides-Shafi string walls, and their spin dynamic response in polar distorted B-phase of ³He. *arXiv preprint arXiv:2008.09286*, 2020.
 - [33] T. W. B. Kibble, G. Lazarides, and Q. Shafi. Walls bounded by strings. *Phys. Rev. D*, 26:435–439, Jul 1982.
 - [34] T.W.B. Kibble, G. Lazarides, and Q. Shafi. Strings in so(10). *Physics Letters B*, 113(3):237 – 239, 1982.
 - [35] T.W. B. Kibble. *Topological Defects and the Non-Equilibrium Dynamics of Symmetry Breaking Phase Transitions*, volume 549. Springer Netherlands, 2000.

- [36] Seji Kang, Sang Won Seo, Hiromitsu Takeuchi, and Y. Shin. Observation of Wall-Vortex Composite Defects in a Spinor Bose-Einstein Condensate. *Phys. Rev. Lett.*, 122:095301, Mar 2019.
- [37] Seji Kang, Deokhwa Hong, Joon Hyun Kim, and Y. Shin. Crossover from weak to strong quench in a spinor Bose-Einstein condensate. *Phys. Rev. A*, 101:023613, Feb 2020.
- [38] Takafumi Kita. Unconventional vortices and phase transitions in rapidly rotating superfluid ^3He -B. *Phys. Rev. B*, 66:224515, Dec 2002.
- [39] M. A. Silaev, E. V. Thuneberg, and M. Fogelström. Lifshitz Transition in the Double-Core Vortex in ^3He -B. *Phys. Rev. Lett.*, 115:235301, Dec 2015.
- [40] Kenichi Kasamatsu, Ryota Mizuno, Tetsuo Ohmi, and Mikio Nakahara. Effects of a magnetic field on vortex states in superfluid ^3He -B. *Phys. Rev. B*, 99:104513, Mar 2019.
- [41] Masaki Tange and Ryusuke Ikeda. Half-quantum vortex pair in the polar-distorted B phase of superfluid ^3He in aerogels. *Phys. Rev. B*, 101:094512, Mar 2020.
- [42] Robert C. Regan, J. J. Wiman, and J. A. Sauls. Vortex phase diagram of rotating superfluid ^3He -B. *Phys. Rev. B*, 101:024517, Jan 2020.
- [43] Subroto Mukerjee, Cenke Xu, and J. E. Moore. Topological Defects and the Superfluid Transition of the $s = 1$ Spinor Condensate in Two Dimensions. *Phys. Rev. Lett.*, 97:120406, Sep 2006.
- [44] A. J. A. James and A. Lamacraft. Phase Diagram of Two-Dimensional Polar Condensates in a Magnetic Field. *Phys. Rev. Lett.*, 106:140402, Apr 2011.
- [45] Michikazu Kobayashi. Berezinskii-Kosterlitz-Thouless Transition of Spin-1 Spinor Bose Gases in the Presence of the Quadratic Zeeman Effect. *Journal of the Physical Society of Japan*, 88(9):094001, 2019.
- [46] D. T. Son and M. A. Stephanov. Domain walls of relative phase in two-component Bose-Einstein condensates. *Phys. Rev. A*, 65:063621, Jun 2002.
- [47] Marek Tylutki, Lev P. Pitaevskii, Alessio Recati, and Sandro Stringari. Confinement and precession of vortex pairs in coherently coupled Bose-Einstein condensates. *Phys. Rev. A*, 93:043623, Apr 2016.
- [48] Minoru Eto and Muneto Nitta. Confinement of half-quantized vortices in coherently coupled Bose-Einstein condensates: Simulating quark confinement in a QCD-like theory. *Phys. Rev. A*, 97:023613, Feb 2018.
- [49] A. Gallemí, L. P. Pitaevskii, S. Stringari, and A. Recati. Decay of the relative phase domain wall into confined vortex pairs: The case of a coherently coupled bosonic mixture. *Phys. Rev. A*, 100:023607, Aug 2019.
- [50] G. M. Fuller, G. J. Mathews, and C. R. Alcock. Quark-hadron phase transition in the early universe: Isothermal baryon-number fluctuations and primordial nucleosynthesis. *Phys. Rev. D*, 37:1380–1400, Mar 1988.
- [51] Kohsuke Yagi, Tetsuo Hatsuda, and Yasuo Miake. *Quark-gluon plasma: From big bang to little bang*, volume 23. Cambridge University Press, 2005.
- [52] Christopher J Pethick and Henrik Smith. *Bose-Einstein condensation in dilute gases*. Cambridge university press, 2008.
- [53] Tetsuo Ohmi and Kazushige Machida. Bose-Einstein condensation with internal degrees of freedom in alkali atom gases. *Journal of the Physical Society of Japan*, 67(6):1822–1825, 1998.
- [54] Haskell B Curry. The method of steepest descent for non-linear minimization problems. *Quarterly of Applied Mathematics*, 2(3):258–261, 1944.
- [55] The details of the numerical method and the cross-section profiles for different values of q/μ are demonstrated in the supplemental material. .
- [56] Neglecting the spin interaction with $\frac{c_1}{c_0} = 0.016 \ll 1$, the critical value is determined $qc/\mu \approx 0.25$ by regarding $\Phi_{\pm 1}$ as a single particle wave function bounded by the vortex core of Φ_0 . A similar problem is solved for the nematic-spin vortex in the AF phase [57]. .
- [57] Andrew P. C. Underwood, D. Baillie, P. Blair Blakie, and H. Takeuchi. Properties of a nematic spin vortex in an antiferromagnetic spin-1 Bose-Einstein condensate. *Phys. Rev. A*, 102:023326, Aug 2020.
- [58] I Liu, Shih-Chuan Gou, Hiromitsu Takeuchi, et al. Phase Diagram of Solitons in the Polar Phase of a Spin-1 Bose-Einstein Condensate. *Phys. Rev. Research*, in press (2020); *arXiv preprint arXiv:2002.06088*, 2020.
- [59] A similar rule has been introduced in the absence of the quadratic Zeeman effect; Tomoya Isoshima, Kazushige Machida, and Tetsuo Ohmi, *Quantum Vortex in a Spinor Bose-Einstein Condensate*, J. Phys. Soc. Jpn. **70**, 1604 (2001) .
- [60] Louis Melville Milne-Thomson. *Theoretical aerodynamics*. Courier Corporation, 1973.
- [61] The details of the derivation of the hydrodynamic potential is described in the supplemental material. .
- [62] A similar behavior was also found in the continuous phase transition of the core state of soliton and vortex in spinor BECs [57, 58] .
- [63] The details of the computation of the spin interaction is described in the supplemental material. .
- [64] Lev Davidovich Landau, Evgenij Mihajlovič Lifšic, Evgenii Mikhailovich Lifshitz, and LP Pitaevskii. *Statistical physics: theory of the condensed state*, volume 9. Butterworth-Heinemann, 1980.
- [65] If $|\Omega|$ exceeds a critical value, vortices are nucleated at the boundary or the core size becomes compared with the system size. .
- [66] G Volovik. Half-quantum vortices in superfluid ^3He -B. *JETP Lett*, 52(6), 1990.
- [67] Y. Kondo, J. S. Korhonen, M. Krusius, V. V. Dmitriev, E. V. Thuneberg, and G. E. Volovik. Combined spin-mass vortex with soliton tail in superfluid ^3He -B. *Phys. Rev. Lett.*, 68:3331–3334, Jun 1992.
- [68] Olli V. Lounasmaa and Erkki Thuneberg. Vortices in rotating superfluid ^3He . *Proceedings of the National Academy of Sciences*, 96(14):7760–7767, 1999.
- [69] Kenichi Kasamatsu, Makoto Tsubota, and Masahito Ueda. Vortex Molecules in Coherently Coupled Two-Component Bose-Einstein Condensates. *Phys. Rev. Lett.*, 93:250406, Dec 2004.
- [70] Mattia Cipriani and Muneto Nitta. Crossover between Integer and Fractional Vortex Lattices in Coherently Coupled Two-Component Bose-Einstein Condensates. *Phys. Rev. Lett.*, 111:170401, Oct 2013.
- [71] Luca Calderaro, Alexander L. Fetter, Pietro Massignan, and Peter Wittek. Vortex dynamics in coherently coupled Bose-Einstein condensates. *Phys. Rev. A*, 95:023605, Feb 2017.
- [72] Kousuke Ihara and Kenichi Kasamatsu. Transverse instability and disintegration of a domain wall of a relative phase in coherently coupled two-component Bose-

Einstein condensates. *Phys. Rev. A*, 100:013630, Jul 2019.

- [73] Michikazu Kobayashi, Minoru Eto, and Muneto Nitta. Berezinskii-Kosterlitz-Thouless Transition of Two-Component Bose Mixtures with Intercomponent Josephson Coupling. *Phys. Rev. Lett.*, 123:075303, Aug 2019.

SUPPLEMENTAL MATERIAL

Method of the numerical simulation

Here, we describe the method of numerical simulation used in this work. The numerical solutions is obtained by minimizing the energy functional

$$G'' = \int_{-R_1}^{R_1} dx \int_{-R_2}^{R_2} dy \int_{-R_3}^{R_3} dz d^3x (\mathcal{G} + V_{\text{trap}}n - \Omega l_z)$$

with the trapping potential V_{trap} and $l_z = \hbar \sum_m \Re[\Phi_m x \partial_y \Phi_m - y \partial_x \Phi_m]$. The space coordinates $(x, y, z) = (x_1, x_2, x_3)$ are discretized as $x_i(n_i) = -R_i + \Delta x n_i$ with $n_i = 0, 1, 2, \dots, N_i$ with $x_i(N_i) = R_i$. The spatial derivatives of Φ_m are computed with finite difference approximation; e.g., $\partial_x \Phi_m$ and $\partial_x^2 \Phi_m$ are computed by the central difference of the first and second order, respectively.

All solutions were obtained by minimizing the energy functional very carefully. The steepest descent method is performed by solving the imaginary time evolution $\frac{\partial \Phi_m}{\partial \tau} = -\frac{\delta G''}{\delta \Phi_m}$. The imaginary time τ is discretized as $\tau = \Delta \tau n_\tau$ with $n_\tau = 0, 1, 2, \dots$. The time evolution is written as $\Phi_m(n_\tau + 1) = \Phi_m(n_\tau) - \Delta \tau \frac{\delta G''}{\delta \Phi_m}(n_\tau)$. The evolutions were computed until the difference $G''(n_\tau) - G''(n_\tau - 1000)$ becomes non-negative within the double precise by using Intel[®] Fortran Compiler.

The solutions in a uniform system is approximately obtained in a cylindrical box potential $V_{\text{trap}} = V_0[\tanh(r - R) + 1]$ with $V_0/\mu = 20$, $R = 0.95R_\perp$, and $R_1 = R_2 = R_\perp$. Here, we solve two-dimensional equations by assuming that the wave functions are homogeneous along the z -axis and thus independent of z . The trap depth V_0 is taken to be so large that the order parameter damps quickly outside the cylinder and almost vanish nearby the system boundary. The boundary effect becomes significant only when the distance l_{spin} between the spin spots becomes $\gtrsim R_\perp/2$. The system size is set to be enough large to neglect the boundary effect for the results in the main text. For the non-rotating case of $\Omega = 0$ (the results of Figs. 1 and 2), the numerical simulation was done with $2R_\perp = 1024.5\xi_n$ with $N_1 = N_2 = 2048$, $\Delta x = 0.5\xi_n$, and $\Delta \tau = 0.0025$. It was confirmed that our results do not change essentially for $\Delta x = 0.3\xi_n$ and $\Delta x = 0.4\xi_n$ except for the finite-size effect, which is of no interest to our main subject. The finite-size effect becomes important only for $\frac{q}{\mu} \leq 2^{-19} \approx 1.9 \times 10^{-6}$ for $\Delta = 0.5\xi_n$. For very small values of $\frac{q}{\mu}$ the width of the elliptic vortex become on the order of or larger than the system size and we could not obtain the vortex state.

The vortex solutions were obtained for $q/\mu = 2^{-n_q}$ ($n_q = 0, 1, 2, \dots$) as shown in Fig. A1. The vortex has the normal core with $\Phi_{\pm 1} = 0$ for $n_q < 3$ (not shown). The protocol of the numerical simulation is as follows. First, the solution for $n_q = 3$ is obtained. Then, the ini-

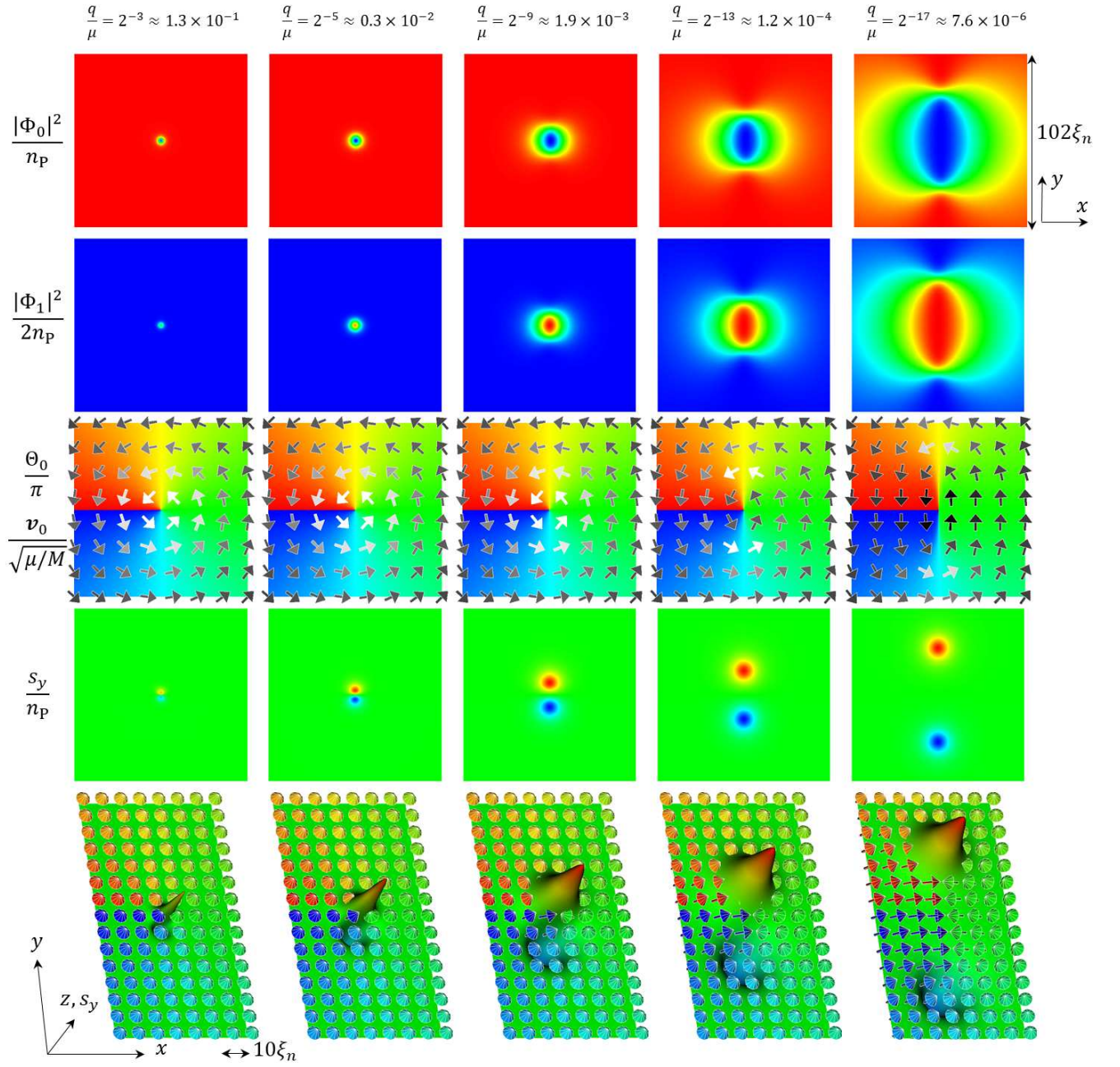


FIG. A1. The cross-sectional profiles of elliptic vortices and the three dimensional texture of pseudo-director field $\mathbf{d}/|\mathbf{d}|$ for $q = 2^{-n_q}$ ($n_q = 3, 5, 9, 13, 17$). The method of plot is the same as that of Fig. 1 in the main text. The angle of view is changed from that in Fig. 1 in the three dimensional plots in the bottom.

tial state of the time evolution is set as $\Phi_0 = f_0(r)e^{i\varphi}$ and $\Phi_{\pm 1} = f_{\pm 1}$ with $f_0(r) = \sqrt{\max(0, \mu - V_{\text{trap}} - \frac{\hbar^2}{2Mr^2})}$ and $f_{\pm 1}(r) = \pm \sqrt{\frac{n_F}{2}} e^{-r^2/\xi_n^2}$. The vortex can be stabilized in the center region even for the non-rotating case of $\Omega = 0$ since the spatial gradient of V_{trap} is negligibly small there. The solution for $n_q + 1$ is obtained by using the solution of n_q as the initial state.

The rotating case of Fig. 3 (a) is obtained with $2R_{\perp} = 410\xi_n$ with $N_1 = N_2 = 1048$ and $\Delta = 0.4\xi_n$. The pro-

ocol is the same as the non-rotating case. For the three dimensional simulation in the harmonic trap of Fig. 3 (b), the system size is $2R_{\perp} = 192.5\xi_n$ and $2R_z = 128.5\xi_n$ with $N_1 = N_2 = 384$, $N_3 = 256$ and $\Delta = 0.5\xi_n$. In the local density approximation, the effective chemical potential is written as $\mu' = \mu - V_{\text{trap}}$. According to Fig. 2(b), the spin density decreases with q/μ' . This is why the spin poles becomes thinner as they are away from the trap center. The vortex core size becomes thicker as the local healing length $\frac{\hbar}{\sqrt{M\mu'}}$ becomes larger for large $|z|$.

Computation of the hydrodynamic potential

The velocity field $\mathbf{v} = (u, v)^T$ in a two dimensional potential flow is represented as $u = \partial_y \Psi = \partial_x \Phi$ and $v = -\partial_x \Psi = \partial_y \Phi$ with the Stream function Ψ and the velocity potential Φ . The complex velocity potential $W = \Phi + i\Psi$ of a point vortex with a circulation Γ in the complex plane (x, y) is written as $W = -i\frac{\Gamma}{2\pi} \log z$. The Joukowski transformation $z = \zeta + \frac{a^2}{\zeta}$ with $\zeta = ae^{\phi+i\psi}$ reads $x = 2a \cosh \phi \cos \psi$ and $y = 2a \sinh \phi \sin \psi$. This transformation corresponds to a mapping from a circle of radius a to an ellipse of major radius $2a \cosh \phi$ and minor radius $2a \sinh \phi$ ($\phi \geq 0$) in the xy -plane. The ellipse reduces a segment of length $4a$ along the x -axis for $\phi = 0$. The segment is along the y -axis if a is replaced by ia in the formula of ζ . We used the formula $\zeta = ae^{\phi+i\psi}$ in the following computation without loss of generality.

In a quantized vortex in a scalar superfluid, the velocity field diverges at the center of the vortex core, where the order parameter amplitude vanishes at the core. The density increases to the bulk value far from the core. The region within a circle of a radius ξ_n with small density around the center is called the core region. To evaluate the energy of a quantized vortex per unit length, the contributions from the core region ($r < \xi_n$) and its outer region ($r > \xi_n$) is computed separately. Similarly, for the elliptic vortex, there exists the core region of an elliptic form around the band-shaped singularity and the energy is computed separately.

To compute the energy analytically, we neglect the so-called quantum pressure term in the Thomas-Fermi (TF) approximation [52]. Then, the density far from the vortex core can be written as

$$n \approx n_{\text{TF}} = n_{\text{bulk}} \left(1 - \frac{M}{2\mu} \mathbf{v}^2 \right)$$

with $n_{\text{bulk}} = n_{\text{P}}$ is the bulk density. In this approximation, one obtains the contribution to the energy functional G from the outer region of area S_{out} up to the order of $\mathcal{O}\left(\frac{M}{2\mu} \mathbf{v}^2\right)$,

$$\begin{aligned} E_{\text{out}} &= \int_{S_{\text{out}}} d^2x \mathcal{G} \\ &\approx \int_{S_{\text{out}}} d^2x \left[\frac{Mn_{\text{TF}}}{2} \mathbf{v}^2 + \mathcal{U}(n_{\text{TF}}) \right] \\ &= \int_{S_{\text{out}}} d^2x \left[\frac{Mn_{\text{P}}}{2} \mathbf{v}^2 + \mathcal{U}_{\text{P}} \right]. \end{aligned} \quad (\text{A1})$$

Here, $\mathcal{U}(n_{\text{TF}})$ is the energy density \mathcal{U} evaluated in the TF approximation, and it reduces to, for the bulk in the P state,

$$\mathcal{U}_{\text{bulk}} = \mathcal{U}_{\text{P}} = -\frac{\mu^2}{2c_0}.$$

A state, different from the P state, appears in the core region where the $m = 0$ component vanishes. The contribution from the core region is written as

$$E_{\text{core}} = \mathcal{U}_{\text{core}} S_{\text{core}}$$

with the energy density $\mathcal{U}_{\text{core}}$ and the area S_{core} of the core region.

The vortex energy E_{vortex} is defined as an excess energy in the presence of the vortex, the difference between the total energy with a vortex and the energy $E_{\text{bulk}} = \mathcal{U}_{\text{bulk}}(S_{\text{core}} + S_{\text{out}})$ in the absence of it;

$$\begin{aligned} E_{\text{vortex}} &= E_{\text{out}} + E_{\text{core}} - E_{\text{bulk}} \\ &= U_{\text{out}} + U_{\text{core}} \end{aligned} \quad (\text{A2})$$

with $U_{\text{core(out)}} = E_{\text{core(out)}} - \mathcal{U}_{\text{P}} S_{\text{core(out)}}$. The potentials of the outer and core regions are rewritten as

$$\begin{aligned} U_{\text{out}} &= \frac{Mn_{\text{bulk}}}{2} \int_{S_{\text{out}}} d^2x \mathbf{v}^2 \\ U_{\text{core}} &= \delta \mu n_{\text{bulk}} S_{\text{core}} \end{aligned} \quad (\text{A3})$$

with $\delta = \frac{\mathcal{U}_{\text{core}}}{\mu n_{\text{bulk}}} + \frac{1}{2}$.

The potential U_{out} , which is reduced to the hydrodynamic potential U_{hyd} as shown later, is evaluated by computing the integral

$$\begin{aligned} I &= \int_{S_{\text{out}}} dx dy \mathbf{v}^2 \\ &= \left(\frac{\Gamma}{2\pi} \right)^2 \int_{S_{\text{out}}} dx dy \left| \frac{1}{\sqrt{z^2 - 4a^2}} \right|^2 \\ &= \left(\frac{\Gamma}{2\pi} \right)^2 \int_{S_{\text{out}}} dx dy \frac{1}{\sqrt{(x^2 - y^2 - 4a^2)^2 + 4x^2 y^2}}. \end{aligned}$$

Here, we used

$$|u| = \frac{\Gamma}{2\pi} \left| \Im \left[\frac{\partial_x \zeta}{\zeta} \right] \right| = \frac{\Gamma}{2\pi} \left| \Im \left[\frac{1}{\sqrt{z^2 - 4a^2}} \right] \right|$$

and

$$|v| = \frac{\Gamma}{2\pi} \left| \Im \left[\frac{\partial_y \zeta}{\zeta} \right] \right| = \pm \frac{\Gamma}{2\pi} \left| \Re \left[\frac{1}{\sqrt{z^2 - 4a^2}} \right] \right|.$$

According to the transformation (for the ellipse along the x -axis)

$$(x, y) = (2a \cosh \phi \cos \psi, 2a \sinh \phi \sin \psi)$$

we have the determinant of the Jacobian matrix

$$\left| \frac{\partial(x, y)}{\partial(\phi, \psi)} \right| = 2a^2 (\cosh 2\phi - \cos 2\psi).$$

The integral I is computed as

$$\begin{aligned}
I &= \left(\frac{\Gamma}{2\pi}\right)^2 \int_{\phi_{\text{core}}}^{\phi_R} d\phi \int_{-\pi}^{\pi} d\psi \frac{1}{2a^2 \sqrt{(\cosh 2\phi - \cos 2\psi)^2}} \left| \frac{\partial(x, y)}{\partial(\phi, \psi)} \right| \\
&= \frac{\Gamma^2}{2\pi} \int_{\phi_{\text{core}}}^{\phi_R} d\phi \\
&= \frac{\Gamma^2}{2\pi} (\phi_R - \phi_{\text{core}}) \\
&= \frac{\Gamma^2}{2\pi} \ln \frac{\rho_R}{\rho_{\text{core}}}
\end{aligned}$$

with the radius of the system boundary in the ζ -plane

$$\rho_R = ae^{\phi_R} \text{ or } \phi_R = \ln \frac{\rho_R}{a}$$

and the cutoff radius for the core region

$$\rho_{\text{core}} = ae^{\phi_{\text{core}}} \text{ or } \phi_{\text{core}} = \ln \frac{\rho_{\text{core}}}{a} \quad (\rho_{\text{core}} > a).$$

The system boundary and the cutoff circle in the ζ -plane are mapped into ellipses in the xy -plane. The major and minor radii are written as

$$\begin{aligned}
A_{R,\text{core}} &= 2a \cosh \phi_{R,\text{core}} = \frac{\rho_{R,\text{core}}^2 + a^2}{\rho_{R,\text{core}}} \\
B_{R,\text{core}} &= 2a \sinh \phi_{R,\text{core}} = \frac{\rho_{R,\text{core}}^2 - a^2}{\rho_{R,\text{core}}} \quad (\text{A4})
\end{aligned}$$

and they satisfy the relation

$$A_{R,\text{core}} + B_{R,\text{core}} = 2\rho_{R,\text{core}}.$$

Here, A_{core} and B_{core} correspond to R_+ and R_- in the main text, respectively. In the limit $\frac{\rho_R}{a} \rightarrow \infty$, we have

$$A_R = B_R \rightarrow \rho_R = R$$

with the radius R of the system boundary in the xy -plane.

The size of the core region is parameterized by two parameters, a and

$$r_{\text{core}} \equiv \rho_{\text{core}} - a.$$

Then, we have

$$U_{\text{out}} \approx U_{\text{hyd}} = \frac{Mn_{\text{P}}}{2} \frac{\Gamma^2}{2\pi} \ln \frac{R}{a + r_{\text{core}}}.$$

The area S_{core} of the core region is represented as

$$S_{\text{core}} = \pi A_{\text{core}} B_{\text{core}} = \pi \frac{(a + r_{\text{core}})^4 - a^4}{(a + r_{\text{core}})^2}$$

The oblateness f of the core region is defined as

$$f = 1 - \frac{B_{\text{core}}}{A_{\text{core}}} = \frac{2}{1 + (1 + r_{\text{core}}/a)^2}.$$

For $\frac{r_{\text{core}}}{a} \ll 1$, asymptotic to the limit of the maximum oblateness ($f = 1$), we have

$$A_{\text{core}} \approx 2a, \quad B_{\text{core}} \approx 2r_{\text{core}}$$

and for $\frac{r_{\text{core}}}{a} \gg 1$, asymptotic to the limit of the minimum oblateness ($f = 0$),

$$A_{\text{core}} = B_{\text{core}} \approx r_{\text{core}}.$$

The former limit corresponds to a vortex with a band-shaped core region in three dimensions, called a vortex band. The latter corresponds to a conventional vortex filament with cylindrical core region.

Computation of the spin interaction

The BA state, emerging around the edge of the elliptic vortex, is collateral in the existence of the AF state in the vortex center. Therefore, the magnetization can be associated with the density at the origin $n_{\text{core}} = n(\mathbf{r} = 0)$. According to the mean-field approach in the previous studies [57, 58], a continuous phase transition occurs at a critical point ($q = q_{\text{C}}$) in the core of a topological defect. This approach is also well applicable to our case. We obtain similar behaviors $n_{\text{core}} \propto 1 - \frac{q}{q_{\text{C}}}$ and $s_y^{\text{max}} = \max s_y \propto \sqrt{1 - \frac{q}{q_{\text{C}}}}$. Since the density is asymptotic to n_{AF} far from the critical point for $q \ll q_{\text{C}}$, a quantitative estimation is obtained by

$$n_{\text{core}} \sim n_{\text{AF}} \left(1 - \frac{q}{q_{\text{C}}}\right),$$

which is quantitatively agreed with the numerical result [Fig. 2(b)].

The magnetization is well described with this approach too. The magnetization happens in the two spin spots with $\arg \Phi_0 = \pm\pi$ along the y -axis. Then the local spin density is written as $F_y \sim \pm 2\sqrt{2n_1}|\Phi_0|^2$ with $\Phi_{+1} = -\Phi_{-1} = \sqrt{n_1} \propto \sqrt{n_{\text{core}}}$. The density is almost constant $n \approx n_{\text{P}}$ everywhere for small q and then the maximum value is estimated by the relation between the arithmetic and geometric means with $2n_1 = \frac{n}{2} \approx \frac{n_{\text{core}}}{2}$ and $|\Phi_0|^2 = \frac{n}{2} \approx \frac{n_{\text{P}}}{2}$ as

$$s_y^{\text{max}} \sim \frac{\sqrt{n_{\text{core}} n_{\text{P}}}}{1 + \frac{c_2}{c_0}},$$

where the factor in the denominator comes from the spin interaction in the presence of spin density.

The size r_{spin} of the magnetic spot around the edges grows with the size of the AF-core, $\sim \xi_q$. The spin interaction becomes more important as the magnetic spot grows and the spot size finally reaches the spin healing length, estimated as

$$\xi_s = \frac{\hbar}{\sqrt{M\sigma}}$$

with $\sigma = c_2 n_P$. This crossover behavior of the spot size is described by a simple formula

$$r_{\text{spin}} = \frac{1}{\xi_s^{-1} + C_{\text{spin}} \xi_q^{-1}},$$

with a constant $C_{\text{spin}} \sim \mathcal{O}(1)$. Finally, the spin interac-

tion energy is evaluated as

$$E_{\text{spin}} \sim \frac{1}{2} c_2 (s_y^{\text{max}})^2 \pi r_{\text{spin}}^2 \sim \frac{\pi}{2} \frac{c_2}{c_0} \frac{n_{\text{core}}}{n_P} \left(\frac{r_{\text{spin}}}{\xi_n} \right)^2 \mu n_P \xi_n^2.$$

This formula is well-consistent with the numerical result with $C_{\text{spin}} = 0.8$.